Crystal structure of LpxC from Pseudomonas aeruginosa complexed with the potent BB-78485 inhibitor

Igor Mochalkin, John D. Knafels and Sandra Lightle

Protein Sci. 2008 17: 450-457
Access the most recent version at doi:10.1110/ps.073324108

Crystal structure of LpxC from *Pseudomonas aeruginosa* complexed with the potent BB-78485 inhibitor

IGOR MOCHALKIN,[1] JOHN D. KNAFELS,[1] AND SANDRA LIGHTLE[2]

[1]Pfizer, Inc., Groton, Connecticut 06340, USA
[2]Pfizer, Inc., Chesterfield, Missouri 63017, USA

(RECEIVED October 29, 2007; FINAL REVISION December 5, 2007; ACCEPTED December 7, 2007)

Abstract

The cell wall in Gram-negative bacteria is surrounded by an outer membrane comprised of charged lipopolysaccharide (LPS) molecules that prevent entry of hydrophobic agents into the cell and protect the bacterium from many antibiotics. The hydrophobic anchor of LPS is lipid A, the biosynthesis of which is essential for bacterial growth and viability. UDP-3-*O*-(*R*-3-hydroxymyristoyl)-*N*-acetylglucosamine deacetylase (LpxC) is an essential zinc-dependant enzyme that catalyzes the conversion of UDP-3-*O*-(*R*-3-hydroxymyristoyl)-*N*-acetylglucosamine to UDP-3-*O*-(*R*-3-hydroxymyristoyl)glucosamine and acetate in the biosynthesis of lipid A, and for this reason, LpxC is an attractive target for antibacterial drug discovery. Here we disclose a 1.9 Å resolution crystal structure of LpxC from *Pseudomonas aeruginosa* (*pa*LpxC) in a complex with the potent BB-78485 inhibitor. To our knowledge, this is the first crystal structure of LpxC with a small-molecule inhibitor that shows antibacterial activity against a wide range of Gram-negative pathogens. Accordingly, this structure can provide important information for lead optimization and rational design of the effective small-molecule LpxC inhibitors for successful treatment of Gram-negative infections.

Keywords: active sites; metalloproteins; LpxC; enzyme inhibitors; antibacterial inhibitor; structure

In Gram-negative bacteria, the cell wall is surrounded by an outer membrane comprised of charged lipopolysaccharide (LPS) molecules (Raetz 1986; Gronow and Brade 2001) that prevent entry of hydrophobic agents into the cell and protect the bacterium from many antibiotics, such as erythromycin, vancomycin, and linezolid (Nikaido and Vaara 1985; Vuorio and Vaara 1992; Vaara 1993). The hydrophobic anchor of LPS is lipid A, the biosynthesis of which is essential for bacterial growth and viability (Raetz 1993, 1996; Wyckoff et al. 1998). Given that the bacterial strains containing a defect in Lipid A biosynthesis are remarkably hypersensitive to antibiotics (Nikaido and Vaara 1985; Vuorio and Vaara 1992; Vaara 1993), development of safe and effective antibacterial agents targeting Gram-negative bacteria has been a primary focus of many research groups and organizations (Onishi et al. 1996; Clements et al. 2002; Kline et al. 2002).

The first committed step in biosynthesis of lipid A is the deacetylation of UDP-3-*O*-(*R*-3-hydroxymyristoyl)-*N*-acetylglucosamine by LpxC, a zinc-dependent UDP-3-*O*-(*R*-3-hydroxymyristoyl)-*N*-acetylglucosamine deacetylase (Anderson et al. 1985, 1988, 1993; Young et al. 1995). Mutagenesis, pH dependence, and structural studies have been utilized to examine the mechanism of deacetylation by LpxC leading to the proposal of single acid-base metalloprotease-like and dual acid-base mechanistic

Reprint requests to: Igor Mochalkin, Pfizer, Inc., Eastern Point Road, Groton, CT 06340, USA; e-mail: Igor.Mochalkin@pfizer.com; fax: (860) 715-3149.

Abbreviations: LpxC, UDP-3-*O*-(*R*-3-hydroxymyristoyl)-*N*-acetylglucosamine deacetylase; *ec*LpxC, LpxC from *Escherichia coli*; *aa*LpxC, LpxC from *Aquifex aeolicus*; *pa*LpxC, LpxC from *Pseudomonas aeruginosa*; MIC, minimal inhibitory concentration; RMS, root-mean-square.

Article and publication are at http://www.proteinscience.org/cgi/doi/10.1110/ps.073324108.

models (Hernick and Fierke 2005; Hernick et al. 2005; McClerren et al. 2005). Key active site residues of *Escherichia coli* LpxC (*ec*LpxC) were identified by probing the molecular determinants of binding and substrate-product specificity on the basis of changes in steady-state turnover and product binding affinity (Hernick and Fierke 2006). Residues F192, K239, D224, and H265 were shown to enhance product affinity and reactivity, while residues E78 and D197 destabilize product affinity. Moreover, residues H19, T191, K143, and N162 preferentially enhance catalytic efficiency by stabilizing the bound substrate and destabilizing the bound product. The determined three-dimensional structures of the LpxC variant from *Aquifex aeolicus* (*aaLpxC*) (residues 1–283) in complex with a substrate analog TU-514 (Gennadios et al. 2006), imidazole (Gennadios et al. 2006), UDP (Buetow et al. 2006; Gennadios and Christianson 2006), and certain fatty acids (Whittington et al. 2003; Hernick et al. 2005; Shin et al. 2007) revealed a unique fold, consisting of two homologous domains each containing two α-helices sandwiched by a five-stranded β-sheet. A ~20 Å-deep LpxC active-site cleft was located at the interface of the two domains and contained a HKXXD zinc-binding motif and a hydrophobic tunnel formed by a βαβ subdomain inserted between β-strand 4 and α-helix A (Whittington et al. 2003). A catalytic zinc ion at the base of the cleft was in a square-pyramidal coordination by a solvent molecule and residues H79, H238, and D242 of *aa*LpxC. An inhibitory zinc ion bound in the presence of excess zinc to residue E78 and H265 and a myristoyl fatty acid that extended into the hydrophobic tunnel. The tunnel is required for efficient catalysis (Jackman et al. 1999; Whittington et al. 2003) and can accommodate a long (C14) fatty acid side chain attached to the *N*-acetylglucosamine group of the substrate. While the myristoyl fatty acid can mimic, to some degree, the fatty acid side chain of the substrate, the binding mode of the UDP moiety of the substrate has not been fully characterized. The reported structures of *aa*LpxC with UDP indicated that the nucleotide can bind in two different conformations (Buetow et al. 2006; Gennadios and Christianson 2006). What binding mode of UDP is biologically relevant for binding of the substrate is not known, since a crystal structure of the substrate complex has not been determined.

While the substrate analogs of LpxC, such as TU-514 (Jackman et al. 2000) and compound **1** (Shin et al. 2007), can bind and inhibit the enzyme, the physical and chemical properties of these compounds make them unattractive candidates for the development of drug-like inhibitors for antibacterial therapy (Scheme 1).

As the search for antibacterial agents intensified, the first synthetic small-molecule inhibitors of LpxC were reported by scientists from Merck (Onishi et al. 1996). These inhibitors contained a hydroxamic acid attached to the 2-phenyloxazoline ring system that can be decorated by methoxy or certain other electron-donating groups to

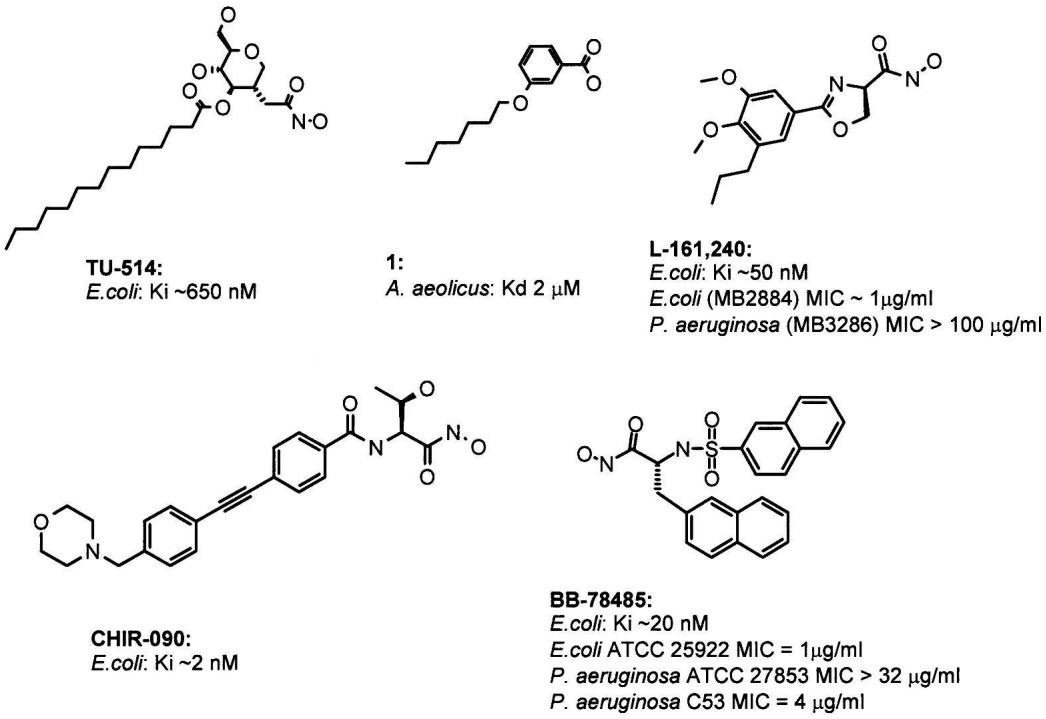

Scheme 1.

enhance potency. Optimization of the series resulted in L-161,240, a potent inhibitor of *ec*LpxC that inhibited growth of the bacteria. However, this compound had no effect on the growth of *Pseudomonas aeruginosa* or *Serratia*, and showed 50- to 100-fold weaker in vitro activity toward the *P. aeruginosa* LpxC enzyme (*pa*LpxC) (Onishi et al. 1996). Following the success of Merck, development of novel compounds targeting *P. aeruginosa* were reported by scientists at Chiron Corporation (Kline et al. 2002) and British Biotech Pharmaceuticals (Clements et al. 2002). The Chiron compounds contain the zinc-binding hydroxamic acid group linked to an aromatic moiety by a heterocyclic or a peptide linker. The most potent reported inhibitors optimized using the Chiron series have K_i values of the ~100 nM range against the isolated *pa*LpxC enzyme and inhibit *E. coli* growth at minimal inhibitory concentrations (MICs) ranging from 1.25 to 12.5 μg/mL (Kline et al. 2002). The sulfonamide derivatives of hydroxamic acid were discovered by British Biotech Pharmaceuticals using screening of a proprietary metalloenzyme inhibitor library (Clements et al. 2002). This series of compounds exemplified by BB-78485 demonstrated antibacterial activity against a wider panel of Gram-negative pathogens, including *Enterobacteriaceae*, *Haemophilis influenzae*, *Serratia marcescens*, and *Burkholderia* (Clements et al. 2002). Although no antibacterial activity was seen against wild-type *Pseudomonas aeruginosa*, some activity of BB-78485 was reported for a semipermeable *P. aeruginosa* bacterial strain, suggesting that access to the target, rather than lack of LpxC inhibitory activity, limited the potency (Clements et al. 2002). Despite the rigorous optimization efforts of the LpxC inhibitors against *P. aeruginosa*, the three-dimensional structure of the *pa*LpxC enzyme has not been reported. Here, we report a 1.9 Å resolution X-ray crystal structure of *P. aeruginosa* LpxC (residues 1–299, C40S) in a complex with the potent BB-78485 inhibitor. To our knowledge, this is the first crystal structure of LpxC with a small-molecule inhibitor that shows antibacterial activity against a wide range of Gram-negative pathogens. Accordingly, this structure can provide important information for lead optimization and rational design of the effective small-molecule LpxC inhibitors for successful treatment of Gram-negative infections.

Results and Discussion

Overall structure of paLpxC

The final *pa*LpxC structure complexed with BB-78485 converged at *R*-work/*R*-free of 0.177/0.221 at resolution 1.9 Å and consisted of 6915 protein atoms, 30 ligand atoms, seven zinc ions, two sulfate ions, and 1223 water molecules. The overall structure was comprised of two α + β domains, each consisting of two primary α-helices and a five-stranded β-sheet (Fig. 1A). The domains were arranged together via packing of the α-helices against each other to form the interior of the protein, which was sandwiched from each end by the β-sheet. Each asymmetric unit contained three protein molecules (Fig. 1B/I) related by a non-crystallographic threefold rotation axis, while in solution *pa*LpxC exists as monomer. In the crystal, an average accessible surface area of the LpxC monomer and an average interface area calculated as an accessible surface area of the interfacing LpxC molecules using *PISA* (Krissinel and Henrick 2007) are 13,074.6 Å^2 and 596.7 Å^2, respectively. Three *pa*LpxC molecules of the homotrimer were almost identical, which especially applied to the active site region. The root-mean-square (RMS) deviations between the superimposed Cα atoms

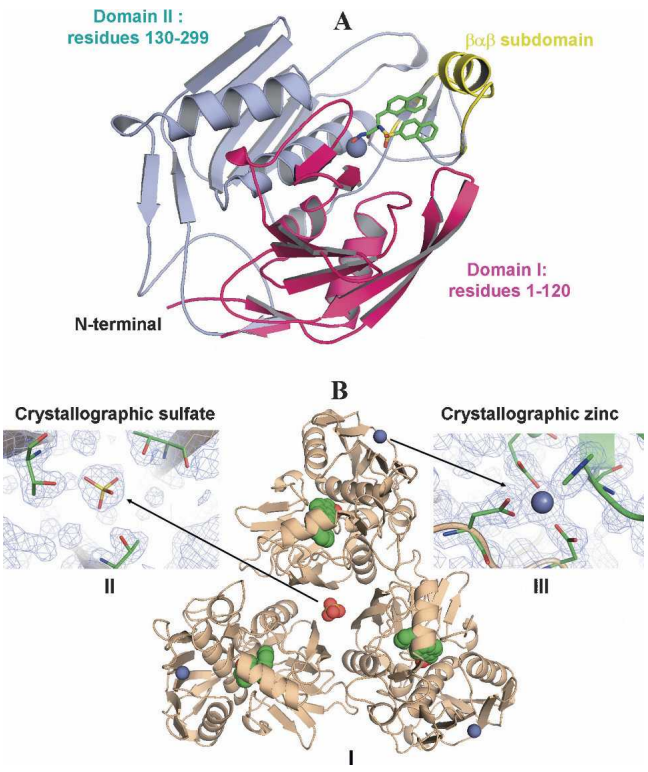

Figure 1. Ribbon representation of the overall structure of *pa*LpxC in complex with BB-78485. (*A*) LpxC domain consists of two homologous domains I (colored in magenta) and II (colored in pink) with an active site and a hydrophobic tunnel located at the interface of the domains. The hydrophobic tunnel is formed by a βαβ subdomain (colored in gold). The BB-78485 molecule is colored in the following atom colors: carbon, green; nitrogen, blue; oxygen, red; sulfur, yellow. Catalytic Zn^{2+} is in purple. (*B*) View of the LpxC/BB-78485 trimer (diagram I) with the final (2Fo–Fc) density maps contoured around a crystallographic sulfate ion (diagram II) and a zinc ion (diagram III) bound at the interface in the LpxC monomers in the trimer. Maps are contoured at the 2.5σ level. Key LpxC residues that interact with the ions are in sticks.

were 0.322 Å (monomers A and B), 0.438 Å (monomers A and C), and 0.307 Å (monomers B and C). The protein had excellent geometry as defined by PROCHECK (Laskowski et al. 1993). The Ramachandran plot generated using final coordinates indicated a close coupling of the ϕ–ψ angles of the residues of the trimer. The Ramachandran plot showed that 701 (89.9%) residues of the total 780 non-glycine and non-proline residues were in most favorable regions, while 76 (9.7%) residues occupied additionally allowed areas. Similar to the *aa*LpxC structure (Whittington et al. 2003), one residue, M103 (L104 in *aa*LpxC), was located in the middle of a β-turn-iil motif with ϕ ~55° and ψ ~120° and in a generously allowed region of the Ramachandran plots. Notwithstanding, the residue had well-defined main- and side-chain electron density. There were no residues in the disallowed region.

A distinguishing characteristic of the LpxC/BB-78485 crystals was the presence of a sulfate group and three Zn^{2+} ions located at the interface of the LpxC molecules (Fig. 1B). The sulfate group was coordinated on the non-crystallographic threefold rotation axis by an extended network of water molecules and the hydrogen-binding contacts (<3.0 Å) with a side-chain oxygen atom of T14 of each LpxC monomer. The average isotropic temperature factor of the refined sulfate group was 38.3 $Å^2$, with atoms occupancy set to 1.0. Three crystallographic zinc ions were located in the homotrimer on the interfaces between pairs of LpxC monomers. The *pa*LpxC residues involved in the interactions with the Zn^{2+} ions were different from those interacting with the crystallographic zinc ion in the *aa*LpxC structure (Whittington et al. 2003). In the *pa*LpxC structure, each zinc ion was in a tetrahedral coordination by the side-chain atoms of D159 and D161 of one LpxC monomer and the residues H162 and E219 of another (Fig. 1B/III). The refined isotropic temperature factors of Zn^{2+} were 17.8 $Å^2$, 19.9 $Å^2$, and 18.9 $Å^2$ for the zinc ions located between monomers A and B, B and C, and A and C, respectively. Because of the important role of zinc and sulfate in intermolecular interactions of LpxC, concentrations of both ions in the cryo-protecting solution significantly affected quality and mosaicity of the frozen crystals.

The overall *pa*LpxC coordinates are similar to the previously reported structure of LpxC from *Aquifex aeolicus* (PDB code: 1p42), monomer A of which was used as an initial protein model in the molecular replacement search (Fig. 2A). Superposition of the refined *pa*LpxC coordinates of monomer A and those of the starting model using secondary structure matching algorithms (Krissinel and Henrick 2004) resulted in an RMS deviation of 1.27 Å on the alignment length of 258 residues. Electron density is well-defined for most of the *pa*LpxC residues of the main chain, except for residues S295–P299 in monomer A and residues A289–P299 in monomer B. Electron density of all (1–299) residues of monomer C is well defined. When compared with the crystal structures of *aa*LpxC (Whittington et al. 2003; Gennadios et al. 2006), the C terminus of the *pa*LpxC variant contains extra 19 residues (W281–P299), which are involved in the formation of an antiparallel β-sheet with the residues K127–I131 (Fig. 2A). A longer C-terminal end of *pa*LpxC, perhaps, provides additional stability of the overall structural fold and enhances crystallizability of the enzyme. Also, the ordered C terminus of *pa*LpxC can, perhaps, provide insights into a process of degradation of LpxC in the bacterial cell. The level of LpxC in the cell is controlled by a membrane-bound protease FtsH belonging to the AAA-ATPase family (Ogura et al. 1999; Führer et al. 2006; Okuno et al. 2006). Recently, Führer et al. demonstrated that the C terminus deletions of five and 11 residues could produce FtsH-resistant variants of LpxC that retained full enzymatic activity (Führer et al. 2006). With no crystal structure available for a binary FtsH/LpxC complex, docking of the refined *pa*LpxC structure (monomer C) into the recently published coordinates of FtsH (Bieniossek et al. 2006) may provide insights into the nature of the protein–protein interactions and help to refine a mechanism of LpxC degradation by FtsH.

Binding mode of BB-78485

The electron density of each inhibitor in the LpxC trimer is well defined for all atoms (Fig. 2B). The hydroxamate moiety of BB-78485 binds to the catalytic Zn^{2+} ion in a fashion similar to that of the hydroxamate of TU-514 (Gennadios et al. 2006): Both oxygen atoms of the zinc-binding group lock zinc in a penta-coordinated configuration within an approximate square-pyramidal geometry (Fig. 2C). Most importantly, the angles under which a plane formed by the hydroxamate atoms of BB-78485 and TU-514 intersect the position of Zn^{2+} are almost identical. In addition to zinc coordination, the hydroxamate OH group forms strong hydrogen bonds with the side chains of E77 (~2.5 Å) and H264 (~2.8 Å) (Fig. 2D). The hydroxamate NH group donates a hydrogen bond to H264–NE2 (~3.0 Å) and the carbonyl group of M62 (~3.3 Å). The hydroxamate C=O group of the inhibitor accepts a hydrogen bond from T190–OG (~2.6 Å), mimicking a carbonyl oxygen of the *N*-acetyl group of the bound substrate, an oxygen atom that is not present in the product. In this respect, LpxC inhibitors containing a hydroxamate group exhibit binding characteristics of the LpxC substrate rather than the product, taking advantage of the preferential effect of the residue T190 for the substrate molecule (Hernick and Fierke 2006). Bridging the zinc-binding hydroxamate group with a naphthalene

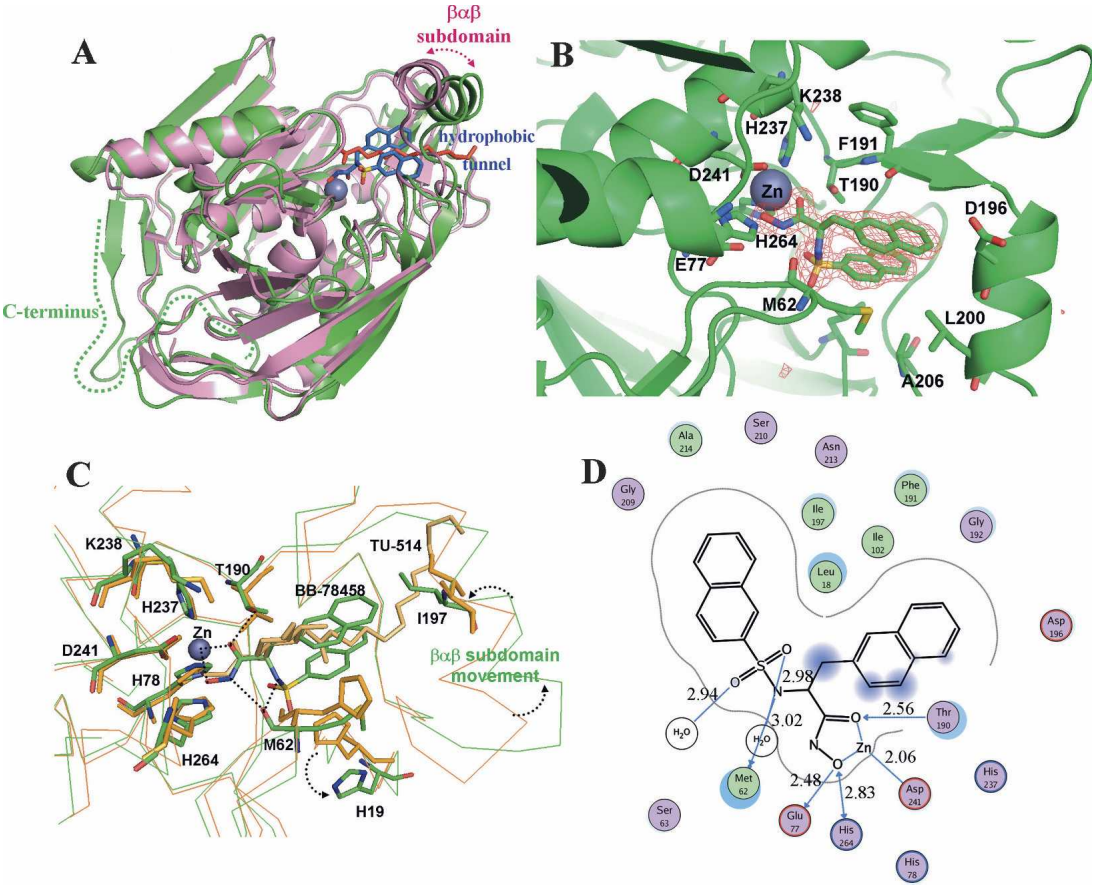

Figure 2. *Pa*LpxC in complex with BB-78485. (*A*) Structural changes at the LpxC active site. Ribbon representation of *pa*LpxC in a complex with BB-78485 is colored in green. The BB-78485 molecule is colored in the following atom colors: carbon, blue; nitrogen, navy blue; oxygen, red; sulfur, yellow. In the BB-78485 complex, the hydrophobic tunnel formed by the βαβ subdomain is in the closed conformation. Ribbon representation of *aa*LpxC in a complex with the myristoyl acid colored in magenta (PDB code 1p42). In the complex with the myristoyl acid that extends into the hydrophobic tunnel, the hydrophobic tunnel is in the open conformation. C-terminal residues 284–299 of *pa*LpxC are highlighted with a dotted line. (*B*) View of the OMIT electron density map contoured at the 3σ level around BB-78485. Key active-site residues involved in the interactions with the inhibitor are shown as sticks. (*C*) View of the superimposed BB-78485 and TU514 (PDB code 1go4, resolution 2.7 Å) at the active site of LpxC. Coordinates of *pa*LpxC/BB-78485 are colored in the following atom colors: carbon, green; nitrogen, blue; oxygen, red; sulfur, yellow. Coordinates of *aa*LpxC/TU-514 are colored in orange. Hydroxamate moieties of BB-78485 and TU-514 bind to the catalytic Zn^{2+} ion in a similar fashion. Movements of the βαβ subdomain and residue H19 are shown with dotted arrows. (*D*) A schematic representation of BB-78485/*pa*LpxC interactions (monomer C) was drawn using the MOE program (Chemical Computing Group, CCG). Hydrophobic residues are colored with a green interior; polar residues are colored in light purple. Basic residues are further annotated by a blue interior ring, and acidic residues with a red ring.

ring system, the sulfonamide linker occupies the bottom of the active site region forming a direct hydrogen bond with the carbonyl oxygen of M62 and several water-mediated interactions with residues T65, E77, S63, and H19. Bridged by the sulfonamide, a naphthalene group makes numerous hydrophobic contacts with the side chain of L18 and the second naphthalene ring system, which is practically in a parallel orientation, in a fashion typical for π−π stacking interactions (Fig. 2B). Except for a similar orientation of the hydroxamate groups, the binding modes of the BB-78485 and TU-514 inhibitors are different resulting in different conformations of the enzyme (Fig. 2C). Briefly, the naphthalene groups of BB-78485 do not penetrate deep into the hydrophobic tunnel, resulting in a complete closure of the tunnel by the movement of the βαβ subdomain. With a completely closed fatty-acid binding cavity, the enzyme appears in a catalytically inactive form which is unable to accommodate a long aliphatic chain of the substrate. In addition, the BB-78485 inhibitor does not occupy a sugar- or UDP-binding region at the top of the active site. In the BB-78485 crystal structure, these regions are occupied by several highly conserved water molecules that form an extensive water network.

Implication to structure-guided drug design

Replacement of hydroxamate in BB-78485 with the alternative zinc-binding groups, such as carboxylic acid, thiadiazole, thiol, thio-ketone, and barbituric acid, resulted in a significant or complete loss of the binding affinity (Clements et al. 2002), suggesting that hydroxamate is a preferred zinc-chelating group for the design of LpxC inhibitors. This is in agreement with the design of amphipathic benzoic acid derivatives (Shin et al. 2007) that showed micromolar or no binding affinity. As BB-78485 and TU-514 structures indicated, the plane formed by the hydroxamate group intersected the location of the catalytic zinc ion under almost identical angles. This suggests that this binding geometry can be used as a restraint for in silico modeling studies of certain types of LpxC inhibitors. However, modeling of CHIR-090 in the refined coordinates of the BB-78485 complex was not successful due to the ''collapsed'' hydrophobic tunnel incapable of accommodating a long biphenyl side chain of the inhibitor, emphasizing high flexibility of the LpxC active site, particularly the hydrophobic tunnel region.

Materials and Methods

Cloning, expression, and purification of the paLpxC

The *pa*LpxC (residues 1–299, C40S) was cloned from genomic DNA by polymerase chain reaction and inserted into pPW4 expression vectors. The recombinant *pa*LpxC was overexpressed in pLysS or AI cells. Cells were collected by centrifugation and frozen at −80°C. The enzyme was purified using a method based on the established protocol (Jackman et al. 2001). Cell paste was resuspended in a buffer containing 10 mM sodium phosphate pH 7.0, 0.1 mM zinc chloride, and 10 mM magnesium chloride in addition to Benzonase (Novagen) and EDTA-free protease inhibitor tablets (Roche). The cell suspension was lysed by two passes through a microfluidizer (Microfluidics Corporation), centrifuged, and the supernatant was decanted. Protein was precipitated by adding ammonium sulfate to 50% saturation, and after centrifugation, the pellet was resuspended in buffer A (10 mM sodium phosphate, pH 7.0). After overnight dialysis against buffer A, protein was loaded onto a DEAE Sepharose ion exchange column equilibrated in buffer A. The enzyme was eluted using a linear gradient from 0–150 mM NaCl. LpxC-containing fractions (as determined by SDS-PAGE) were pooled and loaded onto a Red Sepharose column equilibrated in buffer B (25 mM HEPES, 2 mM TCEP, pH 7.0) + 0.3 M NaCl. Protein was eluted using gradient from 0.3–1.0 M NaCl. LpxC-containing fractions were pooled and concentrated to ~10 mg/mL. Finally, LpxC was loaded onto a Superdex 200 column equilibrated in protein buffer (buffer B + 50 mM NaCl). Pure LpxC fractions were pooled and concentrated to 15 mg/mL and stored at −80°C.

Crystallization and X-ray data collection

Prior to crystallization, *pa*LpxC was diluted to a final concentration of 10 mg/mL in protein buffer with $ZnCl_2$ and BB-78485 added to 1 mM. The mixture was incubated at room temperature for 1 h before crystallization to allow for complex formation. Hanging drops composed of equal volumes of LpxC/BB-78485 and well solution were equilibrated over the well solution at 22°C. The crystals were grown in 0.1 M sodium cacodylate pH 6.5, 0.2 M ammonium sulfate, 10 mM zinc sulfate, and 10% polyethylene glycol 8000. To cryo-protect the crystals, soaking solution containing 16% glycerol in the well solution was slowly added into the crystallization drop before flash-freezing crystals in liquid nitrogen. X-ray diffraction data were collected at the Advanced Photon Source facility beamline 17-ID operated by the Industrial Macromolecular Crystallography Association at about −180°C. The crystal scattered X-rays to 1.9 Å resolution. Auto-indexing and processing of the measured intensities were carried out with the HKL2000 software package (Otwinoski and Minor 1997). The intensity data collection statistics are summarized in Table 1.

Structure determination and refinement

The three-dimensional structure of LpxC with BB-78485 was determined by the molecular replacement method using the Discovery Studio HT-XMR software package (Accelrys, Inc.). The protein coordinates of *aa*LpxC (36% sequence identity) were used as an initial model (PDB code 1p42) (Whittington et al. 2003). Prior to molecular replacement, all residues of *aaLpxC* that were differed in sequence from *pa*LpxC were replaced with the corresponding residues using a model-editing

Table 1. *Data measurement and refinement statistics*

	*pa*LpxC/BB-78485
Data measurement	
Resolution (Å)	34.15–1.90 (1.97–1.90)
Space group	$P2_12_12_1$
Unit cell (Å): *a, b, c*	90.54, 103.33, 105.28
No. of observed reflections	503,911 (43,708)
No. of unique reflections	78,112 (7668)
Completeness (%)	99.9 (99.5)
Multiplicity	6.45 (5.7)
$\langle I/\sigma(I)\rangle$	23.61 (2.5)
R-merge	0.075 (0.524)
No. of atoms	
Protein, chains A/B/C	2306/2272/2340
Inhibitor	30/30/30
Water	1223
Average thermal factor (Å^2)	
Protein, chains A/B/C	26.60/27.42/26.45
Inhibitors	19.2/19.2/21.6
Catalytic zinc ions	22.4/21.3/20.9
Crystallographic zinc ion	17.9/19.9/18.9
Water molecules	38.22
RMS deviation from ideality	
Bond lengths (Å)	0.007
Bond angles (°)	1.122
R-work	0.177
R-free (5% of data)	0.221

Numbers in parentheses indicate statistics for the high-resolution data bin.
R-merge = $\sum hkl\sum i|I(hkl)i - \langle I(hkl)\rangle|/\sum hkl\sum i < I(hkl)i\rangle$.
R-work = $\sum hkl|\mathrm{Fo}(hkl) - \mathrm{Fc}(hkl)|/\sum hkl|\mathrm{Fo}(hkl)|$, where Fo and Fc are observed and calculated structure factors, respectively.

functionality of HT-XMR. The rotation and translation searches were carried out in the range (20.0–3.5) Å resolution that placed three molecules in asymmetric unit and provided the *R*-value of 0.53. The coordinates of the rotated and translated *pa*LpxC trimer were further optimized by rigid-body refinement with each LpxC monomer defined as a rigid-body group followed by coordinates and B-value minimization to decrease the *R*-work/*R*-free values to 0.452/0.483. Two succeeding iterations of automated protein rebuilding using DS HT-XMR further decreased the *R*-values to 0.377/0.443. From this point, three rounds of manual fitting of protein coordinates and zinc ions into electron density using the X-BUILD tools (Oldfield 2001a) in QUANTA (Accelrys Inc.) alternated with simulated annealing refinement using CNX 2002 (Brünger et al. 1998; Accelrys Inc.) and then REFMAC 5.1 (Collaborative Computational Project, Number 4 1994; Murshudov et al. 1997) software programs. The calculated (2Fo–Fc) and (Fo–Fc) electron density maps were utilized for additional manual fitting of protein coordinates to lower the *R*-values to 0.278/0.305. Ligand placement was carried out with QUANTA X-LIGAND (Oldfield 2001b). Solvent water molecules were added based on examination of difference density maps using X-SOLVATE (Accelrys Inc). Summary of final refinement parameters is listed in Table 1.

Data deposition

Atomic coordinates have been deposited in the RCSB Protein Data Bank (accession code: 2ves)

Acknowledgments

The authors thank our fellow colleagues from Pfizer, Inc.: Guru Siradanahalli, Susan Holley, and Loola Al-Kassim for cloning the LpxC enzyme; Craig Banotai and Cindy Spessard for the LpxC expression and scale-up work; W. Tom Mueller for providing advice on LpxC purification protocols; Cheryl Quinn for her leadership and guidance; Karen Leach and Michael Miller for insightful comments on the manuscript. Use of the Advanced Photon Source was supported by the U.S. Department of Energy, Basic Energy Sciences, Office of Science, under Contract No. W-31-109-Eng-38. Access to the IMCA-CAT facilities are supported by the companies of the Industrial Macromolecular Crystallography Association through a contract with Illinois Institute of Technology (IIT), executed through IIT's Center for Synchrotron Radiation Research and Instrumentation.

References

Anderson, M.S., Bulawa, C.E., and Raetz, C.R. 1985. The biosynthesis of Gram-negative endotoxin. Formation of lipid A precursors from UDP–GlcNAc in extracts of *Escherichia coli*. *J. Biol. Chem.* **260:** 15536–15541.

Anderson, M.S., Robertson, A.D., Macher, I., and Raetz, C.R.H. 1988. Biosynthesis of lipid A in *Escherichia coli*: Identification of UDP-3-*O*-[(*R*)-3-hydroxymyristoyl]-α-D-glucosamine. *Biochemistry* **27:** 1908–1917.

Anderson, M.S., Bull, H.G., Galloway, S.M., Kelly, T.M., Mohan, S., Radika, K., and Raetz, C.R.H. 1993. UDP-*N*-acetylglucosamine acetyltransferase of *Escherichia coli*. The first step in endotoxin biosynthesis is thermodynamically unfavorable. *J. Biol. Chem.* **268:** 19858–19865.

Bieniossek, C., Schalch, T., Bumann, M., Meister, M., Meier, R., and Baumann, U. 2006. The molecular architecture of the metalloprotease FtsH. *Proc. Natl. Acad. Sci.* **103:** 3066–3071.

Brünger, A.T., Adams, P.D., Clore, G.M., DeLano, W.L., Gros, P., Grosse-Kunstleve, R.W., Jiang, J.S., Kuszewski, J., Nilges, M., Pannu, N.S., et al. 1998. Crystallography & NMR system: A new software suite for macromolecular structure determination. *Acta Crystallogr.D Biol. Crystallogr.* **D54:** 905–921.

Buetow, L., Dawson, A., and Hunter, W.N. 2006. The nucleotide-binding site of Aquifex aeolicus LpxC. *Acta Crystallogr. Sect. F Struct. Biol. Cryst. Commun.* **F62:** 1082–1086.

Clements, J.M., Coignard, F., Johnson, I., Chandler, S., Palan, S., Waller, A., Wijkmans, J., and Hunter, M.G. 2002. Antibacterial activities and characterization of novel inhibitors of LpxC. *Antimicrob. Agents Chemother.* **46:** 1793–1799.

Collaborative Computational Project, Number 4. 1994. The CCP4 suite: Programs for protein crystallography. *Acta Crystallogr.* **D50:** 760–763.

Führer, F., Langklotz, S., and Narberhaus, F. 2006. The C-terminal end of LpxC is required for degradation by the FtsH protease. *Mol. Microbiol.* **59:** 1025–1036.

Gennadios, H.A. and Christianson, D.W. 2006. Binding of uridine 5′-diphosphate in the "basic patch" of the zinc deacetylase LpxC and implications for substrate binding. *Biochemistry* **45:** 15216–15223.

Gennadios, H.A., Whittington, D.A., Li, X., Fierke, C.A., and Christianson, D.W. 2006. Mechanistic inferences from the binding of ligands to LpxC, a metal-dependent deacetylase. *Biochemistry* **45:** 7940–7948.

Gronow, S. and Brade, H. 2001. Invited review: Lipopolysaccharide biosynthesis: Which steps do bacteria need to survive? *J. Endotoxin Res.* **7:** 3–23.

Hernick, M. and Fierke, C.A. 2005. Zinc hydrolases: The mechanism of zinc-dependent deacetylases. *Arch. Biochem. Biophys.* **433:** 71–84.

Hernick, M. and Fierke, C.A. 2006. Catalytic mechanism and molecular recognition of *E. coli* UDP-3-*O*-(*R*-3-hydroxymyristoyl)-*N*-acetylglucosamine deacetylase probed by mutagenesis. *Biochemistry* **45:** 15240–15248.

Hernick, M., Gennadios, H.A., Whittington, D.A., Rusche, K.M., Christianson, D.W., and Fierke, C.A. 2005. UDP-3-O-((R)-3-hydroxymyristoyl)-N-acetylglucosamine deacetylase functions through a general acid-base catalyst pair mechanism. *J. Biol. Chem.* **280:** 16969–16978.

Jackman, J.E., Raetz, C.R., and Fierke, C.A. 1999. UDP-3-*O*-(R-3-hydroxymyristoyl)-*N*-acetylglucosamine deacetylase of *Escherichia coli* is a zinc metalloenzyme. *Biochemistry* **38:** 1902–1911.

Jackman, J.E., Fierke, C.A., Tumey, L.N., Pirrung, M., Uchiyama, T., Tahir, S.H., Hindsgaul, O., and Raetz, C.R. 2000. Antibacterial agents that target lipid A biosynthesis in Gram-negative bacteria. Inhibition of diverse UDP-3-*O*-(R-3-hydroxymyristoyl)-*N*-acetylglucosamine deacetylases by substrate analogs containing zinc binding motifs. *J. Biol. Chem.* **275:** 11002–11009.

Jackman, J.E., Raetz, C.R.H., and Fierke, C.A. 2001. Site-directed mutagenesis of the bacterial metalloamidase UDP-(3-O-acyl)-N-acetylglucosamine deacetylase (LpxC). Identification of the zinc binding site. *Biochemistry* **40:** 514–523.

Kline, T., Andersen, N.H., Harwood, E.A., Bowman, J., Malanda, A., Endsley, S., Erwin, A., Doyle, M., Fong, S., Harris, A., et al. 2002. Potent, novel in vitro inhibitors of the *Pseudomonas aeruginosa* deacetylase LpxC. *J. Med. Chem.* **45:** 3112–3129.

Krissinel, E. and Henrick, K. 2004. Secondary-structure matching (SSM), a new tool for fast protein structure alignment in three dimensions. *Acta Crystallogr.* **D60:** 2256–2268.

Krissinel, E. and Henrick, K. 2007. Inference of macromolecular assemblies from crystalline state. *J. Mol. Biol.* **372:** 774–797.

Laskowski, R.A., MacArthur, M.W., Moss, D.S., and Thornton, J.M. 1993. PROCHECK: A program to check the stereochemical quality of protein structures. *J. Appl. Crystallogr.* **26:** 283–291.

McClerren, A.L., Zhou, P., Guan, Z., Raetz, C.R.H., and Rudolph, J. 2005. Kinetic analysis of the zinc-dependent deacetylase in the lipid A biosynthesis pathway. *Biochemistry* **44:** 1106–1113.

Murshudov, G.N., Vagin, A.A., and Dodson, E.J. 1997. Refinement of macromolecular structures by the maximum-likelihood method. *Acta Crystallogr. D Biol. Crystallogr.* **D53:** 240–255.

Nikaido, H. and Vaara, M. 1985. Molecular basis of bacterial outer membrane permeability. *Microbiol. Rev.* **49:** 1–32.

Ogura, T., Inoueu, K., Suzaki, T., Karata, K., Young, K., Su, L.H., Fierke, C.A., Jackman, J.E., Raetz, C.R., Coleman, J., et al. 1999. Balanced biosynthesis of major membrane components through regulation degradation of the committed enzyme of lipid A biosynthesis by the AAA protease FtsH (HflB) in *Escherichia coli*. *Mol. Microbiol.* **31:** 833–844.

Okuno, T., Yamanaka, K., and Ogura, T. 2006. Characterization of mutants of the *Escherichia coli* AAA protease FtsH, carrying a mutation in the central pore region. *J. Struct. Biol.* **156:** 109–114.

Oldfield, T.J. 2001a. A number of real-space torsion-angle refinement techniques for proteins, nucleic acids, ligands and solvent. *Acta Crystallogr.* **D57:** 82–94.

Oldfield, T.J. 2001b. X-LIGAND: An application for the automated addition of flexible ligands into electron density. *Acta Crystallogr.* **D57:** 696–705.

Onishi, H.R., Pelak, B.A., Gerckens, L.S., Silver, L.L., Kahan, F.M., Chen, M.H., Patchett, A.A., Galloway, S.M., Hyland, S.A., Anderson, M.A., et al. 1996. Antibacterial agents that inhibit lipid A biosynthesis. *Science* **274:** 980–982.

Otwinoski, Z. and Minor, W. 1997. Processing of X-ray diffraction data collected in oscillation mode. In *Methods in enzymology* (eds. C.W. Carter Jr. and R.M. Sweet), 276(A) ed., pp. 307–326. Academic Press, New York.

Raetz, C.R.H. 1986. Molecular genetics of membrane phospholipid synthesis. *Annu. Rev. Genet.* **20:** 253–295.

Raetz, C.R.H. 1993. Bacterial endotoxins: Extraordinary lipids that activate eukaryotic signal transduction. *J. Bacteriol.* **175:** 5745–5753.

Raetz, C.R.H. (1996) Bacterial lipopolysaccharides: A remarkable family of bioactive macroamphiphiles. In Escherichia coli *and* Salmonella*: Cellular and molecular biology* (ed. F.C. Neidhardt), Vol. 1, 2nd ed., pp. 1035–1063. American Society for Microbiology, Washington, DC.

Shin, H., Gennadios, H.A., Whittington, D.A., and Christianson, D.W. 2007. Amphipathic benzoic acid derivatives: Synthesis and binding in the hydrophobic tunnel of the zinc deacetylase LpxC. *Bioorg. Med. Chem.* **15:** 2617–2623.

Vaara, M. 1993. Outer membrane permeability barrier to azithromycin, clarithromycin, and roxithromycin in gram-negative enteric bacteria. *Antimicrob. Agents Chemother.* **37:** 354–356.

Vuorio, R. and Vaara, M. 1992. The lipid A biosynthesis mutation lpxA2 of *Escherichia coli* results in drastic antibiotic supersusceptibility. *Antimicrob. Agents Chemother.* **36:** 826–829.

Whittington, D.A., Rusche, K.M., Shin, H., Fierke, C.A., and Christianson, D.W. 2003. Crystal structure of LpxC, a zinc-dependent deacetylase essential for endotoxin biosynthesis. *Proc. Natl. Acad. Sci.* **100:** 8146–8150.

Wyckoff, T.J.O., Raetz, C.R.H., and Jackman, J.E. 1998. Antibacterial and anti-inflammatory agents that target endotoxin. *Trends Microbiol.* **6:** 154–159.

Young, K., Silver, L.L., Bramhill, D., Cameron, P., Eveland, S.S., Raetz, C.R.H., Hyland, S.A., and Anderson, M.S. 1995. The envA permeability/cell division gene of *Escherichia coli* encodes the second enzyme of lipid A biosynthesis. UDP-3-*O*-[*R*-3-hydroxymyristoyl]-*N*-acetylglucosamine deacetylase. *J. Biol. Chem.* **270:** 30384–30391.